中国光学（中英文） Chinese Optics 核心期刊

High-precision color crosstalk coefficient calibration method based on phase error estimation

FENG Lu-yuan, LIANG Jian, WANG Xiang-jun, ZHAO Zong-yang, CHEN Yi-fan, WU Bin

Citation:
FENG Lu-yuan, LIANG Jian, WANG Xiang-jun, ZHAO Zong-yang, CHEN Yi-fan, WU Bin. High-precision color crosstalk coefficient calibration method based on phase error estimation[J]. *Chinese Optics*, In press. doi: 10.37188/CO.EN-2025-0041
冯橹源, 梁健, 王湘峻, 赵宗扬, 陈羿帆, 吴斌. 基于相位误差估计的高精度色彩串扰系数标定方法[J]. 中国光学, 优先发表. doi: 10.37188/CO.EN-2025-0041

View online: https://doi.org/10.37188/CO.EN-2025-0041

Articles you may be interested in

文章编号　2097-1842(xxxx)x-0001-09

High-precision color crosstalk coefficient calibration method based on phase error estimation

FENG Lu-yuan[1,2], LIANG Jian[2], WANG Xiang-jun[3], ZHAO Zong-yang[2], CHEN Yi-fan[2], WU Bin[2*]

(1. *China Ordnance Navigation and Control Technology Research Institute*, *Beijing* 100089, *China*;
2. *State Key Laboratory of Precision Measurement Technology and Instruments*, *Tianjin University*, *Tianjin* 300072, *China*;
3. *Dezhou academy of agricultural sciences*, *Shandong* 253015, *China*)

* *Corresponding author*, *E-mail*: *wubin@tju.edu.cn*

Abstract: Color-coded fringe patterns have emerged as a key technique for enabling real-time three-dimensional (3D) shape measurement in fringe projection profilometry (FPP). However, color crosstalk inherent in color cameras remains a significant factor limiting measurement accuracy. To mitigate this issue, a high-precision calibration method for color crosstalk coefficients is proposed to enable effective correction in this paper. Specifically, a crosstalk coefficient estimator is developed based on orthogonal phase-shifted fringe patterns, and the theoretical relationship between the crosstalk coefficients and phase error is derived. The color orthogonal fringes are then designed to project onto a standard planar target to acquire separated R, G, and B channel patterns. Finally, a particle swarm optimization (PSO) algorithm is introduced to optimize the crosstalk-induced phase errors and calibrate the crosstalk coefficients with high precision. Experimental validation based on a standard dual-sphere calibration plate shows that the diameter fitting errors of the two spheres are 0.0191 mm and 0.0160 mm, respectively, and the error in the calculated center-to-center distance is as low as 0.0120 mm, which demonstrate that the proposed method can effectively enhance the measurement accuracy and applicability of color cameras in fringe projection technology.

Key words: Fringe projection profilometry; color crosstalk coefficient; phase error; orthogonal fringe pattern

基于相位误差估计的高精度色彩串扰系数标定方法

冯橹源[1,2], 梁　健[2], 王湘峻[3], 赵宗扬[2], 陈羿帆[2], 吴　斌[2*]

(1. 中国兵器工业导航与控制技术研究所, 北京 100089;
2. 天津大学 精密测试技术及仪器全国重点实验, 天津 300072;
3. 德州市农业科学研究院, 山东 253015)

摘要: 彩色编码条纹图案已成为实现条纹投影轮廓术实时三维形貌测量的重要方法。然而, 彩色相机中的色彩串扰现象

收稿日期: 2025-10-16; **修订日期:** xxxx-xx-xx

基金项目: 国家自然科学基金(No. 62371339)

Supported by National Natural Science Foundation of China (No. 62371339).

仍然是限制测量精度的主要因素。针对这一问题，本文提出了一种精确的色彩串扰系数标定方法，以实现有效的色彩串扰校正。首先，设计了一种基于正交相位条纹的串扰系数估计器，从理论上推到了色彩串扰系数与相位误差的关系。同时，将设计的彩色正交条纹图案投影至标准平面靶标，实现 R、G、B 的彩色通道分离图案。最后，基于粒子群优化算法拟合通道串扰相位误差，从而实现高精度色彩串扰系数标定。基于标准双球球板的测量实验验证，两个球体的直径拟合误差分别为 0.0191 mm 和 0.0160 mm，球心间距的计算误差低至 0.0120 mm，证明该方法能够有效提高彩色相机在条纹投影技术中的测量精度和适用性。

关　键　词：条纹投影轮廓术；色彩串扰系数；相位误差；正交条纹图案

中图分类号：TH741　　**文献标志码：**A　　**doi：**10.37188/CO.EN-2025-0041　　**CSTR：**32171.14.CO.EN-2025-0041

1 Introduction

Nowadays, high-accuracy optical-based three-dimensional (3D) shape measurement has become increasingly important across a wide range of fields, owing to its advantages of non-contact, high resolution and simple system configuration[1-3]. Among the available techniques, color fringe projection profilometry (CFPP) has attracted considerable attention due to its high efficiency and strong robustness[4]. The principle of CFPP involves projecting color fringe patterns onto an object and capturing the reflected images with a color camera, from which phase information is extracted to reconstruct the object's 3D surface, as shown in Fig. 1.

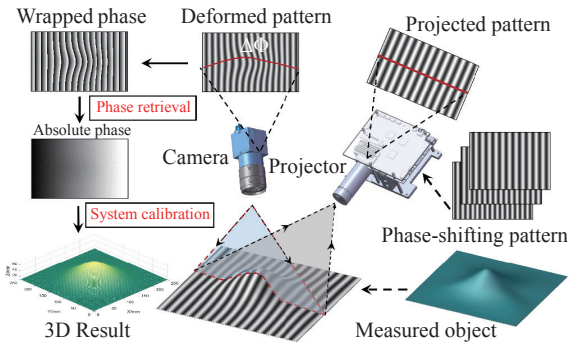

Fig. 1　The schematic of the 3D measurement process based on FPP

图 1　基于 FPP 的三维测量过程示意图

However, color cameras equipped with color filter arrays (CFAs) are prone to significant crosstalk due to overlapping spectral responses between filters, which severely compromises measurement accuracy. This issue is particularly pronounced in systems utilizing Bayer filter arrays, where inter-channel intensity interference leads to errors in phase calculation. As a result, effective separation of signals from different color channels has become a key challenge for achieving high-precision measurements results[5].

To mitigate the effects of color crosstalk, two main strategies have been explored: hardware-based and software-based compensation methods. Hardware solutions, such as the use of three separate filters[6] or color filters with 50% transmittance[7], aim to reduce spectral overlap between channels. However, these approaches often require additional devices, which could increase system complexity and cost. On the other hand, software-based techniques, including crosstalk coefficient calibration[8-9], function -based correction methods[10-11], signal analysis approaches[12-13], and deep learning models[14-15], have also been proposed. Despite their promise, many of these methods demand a large number of projected patterns, extensive datasets, or highly controlled experimental conditions, which limits their practical applicability. Considering the characteristics and applicability of various methods, it is evident that channel crosstalk is primarily determined by the intrinsic properties of the imaging system. Therefore, it can be effectively mitigated through pre-calibration and correction, thereby minimizing its impact on coefficient measurements.

In this study, a high-precision color crosstalk coefficient calibration method is proposed. A crosstalk coefficient estimator is designed based on orthogonal phase-shifted fringe patterns to derive the crosstalk-induced errors in the wrapped phase. Using the theoretical relationship between the crosstalk coefficients and phase error, color ortho-

gonal fringes are then developed to project onto a standard planar target to acquire separated R, G, and B channel patterns. By applying a parameter fitting strategy, the crosstalk coefficients are calibrated and subsequently used for color decoupling. The proposed method delivers highly accurate calibration results while requiring only a low-cost CMOS camera and a simple, easy-to-implement algorithm, making it well suited for fast and flexible calibration scenarios.

The remainder of this paper is organized as follows: Section 2 introduces the error transformation model and the principles of the proposed calibration method; Section 3 presents the experimental results; and Section 4 concludes the paper.

2 Principle of the Proposed Method

2.1 Principle of FPP

In a standard procedure, a series of phase-shifted fringe patterns are generated and projected onto the surface of the object. The resulting deformed fringe images are then captured by the camera. Subsequently, the wrapped phase φ, containing 2π discontinuities and ranging from $-\pi$ to $+\pi$, is computed. To retrieve the continuous full-field phase map Φ, a multi-frequency phase unwrapping algorithm[16] is employed. Following system calibration, the three-dimensional point cloud of the object is reconstructed based on the recovered phase Φ. In this work, a widely adopted phase-shifting algorithm is utilized to obtain the wrapped phase φ, which can be formulated as:

$$I_n(u,v) = A(u,v) + B(u,v)\cos\left[\varphi(u,v) + 2\pi n/N\right], \quad (1)$$

where $n \in [0, N-1)$ denotes the index of the N-step phase-shifted patterns, and N indicates the total number of phase steps. The coordinate pair (u, v) refers to the pixel location on the camera sensor. The parameters A and B represent the average intensity and modulation intensity, respectively. Based on these definitions, the wrapped phase φ can be calculated as:

$$\varphi = -\text{atan2}\left[\sum_{n=0}^{N-1} I_n \sin(2\pi n/N) / \sum_{n=0}^{N-1} I_n \cos(2\pi n/N)\right], \quad (2)$$

2.2 Color crosstalk matrix model

CMOS sensors are extensively employed in color cameras owing to their low cost, high resolution, and capability to meet the requirements of dynamic measurements. The relative spectral response curves and imaging principle of the Bayer array are illustrated in Fig. 2. The Bayer filter array is mounted in front of the CMOS sensor so that individual pixels selectively capture red, green, or blue light. The missing color information at each pixel is subsequently reconstructed through a de-mosaicing algorithm, which interpolates the absent color channels based on data from neighboring pixels[17].

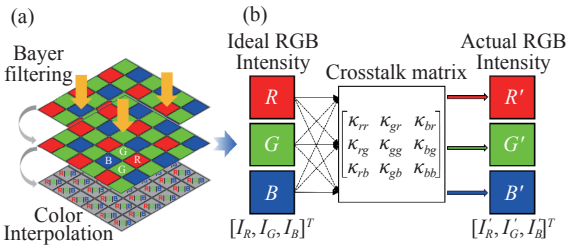

Fig. 2 The schematic of the color crosstalk. (a) the schematic model of Bayer array; (b) the color crosstalk model.

图 2 色彩串扰的示意图。(a) Bayer 阵列的结构模型; (b) 色彩串扰数学模型

However, spectral overlap among the RGB channels is introduced through this process, leading to color crosstalk and resulting in systematic errors during phase computation. As a result, the coupled intensity can be mathematically expressed as:

$$\begin{bmatrix} I'_R \\ I'_G \\ I'_B \end{bmatrix} = K \begin{bmatrix} I_R \\ I_G \\ I_B \end{bmatrix} = \begin{bmatrix} \kappa_{rr} & \kappa_{gr} & \kappa_{br} \\ \kappa_{rg} & \kappa_{rr} & \kappa_{bg} \\ \kappa_{rb} & \kappa_{rg} & \kappa_{rr} \end{bmatrix} \begin{bmatrix} I_R \\ I_G \\ I_B \end{bmatrix}, \quad (3)$$

where I'_R, I'_G, and I'_B are interpreted as the actual intensities of the red, green, and blue channels, respectively. Correspondingly, I_R, I_G, and I_B denote the ideal intensities. The term κ_{st} (where s, $t = r$, g, b) represents the crosstalk influence coefficient from channel s to channel t, with $\kappa_{st} = 1$ (where $s = t$) in-

dicating the self-channel response. Once the crosstalk matrix κ is calibrated, the ideal channel intensities can be recovered through inverse computation as follows:

$$[I_R, I_G, I_B]^T = inv(\kappa)[I'_R, I'_G, I'_B]^T \quad , \qquad (4)$$

2.3 Crosstalk coefficient estimation

A set of orthogonal fringe patterns is designed to establish a crosstalk estimation framework in this paper. The crosstalk matrix κ is subsequently identified by analyzing the phase errors induced by color crosstalk. Initially, angular information is introduced into the phase-shifted fringe patterns. The sinusoidal fringe pattern incorporating the angular parameter θ is defined as:

$$I_n(u,v,\theta) = A(u,v) + B(u,v)\cos[2\pi(u\sin\theta + v\cos\theta)/T + \delta_i] \quad , \qquad (5)$$

where T is the fringe period; $\delta_n = 2\pi n/N$ corresponds to the phase shift of the n-th step in the N-step phase-shifting method; and $\theta \in [0,\pi)$ defines the angle between the fringe orientation and the horizontal axis.

To simplify the calibration process, channel pairs are grouped and calibrated using orthogonal fringe patterns. This yields intensity values that contain crosstalk effects, which can be expressed as:

$$I_n^{st}(u,v,\theta_1) = I_n^s(u,v,\theta_1) + \kappa_{st} I_n^t(u,v,\theta_2) \quad , \qquad (6)$$

where I_n^{st} denotes the actual intensity captured under the angular configuration θ_1, extracted from the orthogonal fringe patterns. This indicates that the signal in channel s contains crosstalk originating from channel t. The angular relationship is defined as $\theta_1 = \theta_2 + \pi/2$, corresponding to a pair of orthogonal directions.

Due to the interference fringe, the resulting intensity becomes a mixture of two sinusoidal components with slightly different frequencies or orientations. The result could deviate from the ideal phase when four-step phase-shifting method is used to extract the phase from this mixed signal.

The extracted wrapped phase from the crosstalk-affected signal φ_{st} and the ideal signal φ_s are compared to quantify this deviation. By analyzing the phasor composed of the crosstalk component as an additional term in the complex plane, the phase deviation can be derived as:

$$\varphi_{st}(u,v) = \arctan\left\{\frac{\sin[2\pi(u\sin\theta_1 + v\cos\theta_1)/T] + \kappa_{st}\sin[2\pi(u\sin\theta_2 + v\cos\theta_2)/T]}{\cos[2\pi(u\sin\theta_1 + v\cos\theta_1)/T] + \kappa_{st}\cos[2\pi(u\sin\theta_2 + v\cos\theta_2)/T]}\right\} \quad , \qquad (7)$$

$$\varphi_s(u,v) = \arctan\left\{\frac{\sin[2\pi(u\sin\theta_1 + v\cos\theta_1)/T]}{\cos[2\pi(u\sin\theta_1 + v\cos\theta_1)/T]}\right\} \quad , \qquad (8)$$

$$\Delta\varphi_s(u,v) = \varphi_{st}(u,v) - \varphi_s(u,v) = \arctan\left\{\frac{\kappa_{st}\sin[2\pi(u\sin\theta_2 + v\cos\theta_2)/T - 2\pi(u\sin\theta_1 + v\cos\theta_1)/T]}{1 + \kappa_{st}\cos[2\pi(u\sin\theta_2 + v\cos\theta_2)/T - 2\pi(u\sin\theta_1 + v\cos\theta_1)/T]}\right\}, \qquad (9)$$

where φ_{st} represents the phase affected by crosstalk, and φ_s denotes the reference phase obtained without crosstalk, which is measured using a 12-step phase-shifting method with a single-color channel. Given that $\theta_1 = \theta_2 + \pi/2$ and the crosstalk coefficient κ_{st} is typically small, a Taylor series expansion[18] can be applied to simplify the Eq.(9), which could be expressed as:

$$\Delta\varphi_s(u,v) \approx \kappa_{st}\sin[2\pi u(\sin(\theta_2) + \cos(\theta_2))/T - 2\pi v(\cos(\theta_2) - \sin(\theta_2))/T] \quad , \qquad (10)$$

It is worth noting that the terms $2\pi u/T$ and $2\pi v/T$ and in Eq. (10) represent the phase components along directions θ_1 and θ_2, respectively. This two-dimensional sinusoidal model captures the spatial variation of the phase error, which inherently follows a periodic pattern due to the sinusoidal nature of the fringe projection. Based on the derived relationship, once the phase error map is obtained, the parameters κ_{st} and θ_1 can be estimated by fitting the error distribution to Eq. (10). In this study, the Particle Swarm Optimization (PSO) method[19] is employed for parameter fitting, as it is

well suited for solving multi-dimensional optimization problems and handling complex continuous functions with multiple local minima.

The derivation of Eq. (9) is valid only under a specific condition, as defined in Eq. (11). However, some data points do not satisfy this requirement, leading to non-sinusoidal characteristics in the resulting phase error distribution. To illustrate this effect, a segment of the wrapped phase error is extracted when $\kappa_{st} = 0.1$, as shown in Fig. 3. For the points that violate the condition, the use of the atan2 function introduces phase discontinuities of -2π or $+2\pi$, which degrade the accuracy of coefficient fitting. To address this issue, a compensation of $\pm 2\pi$ should be applied to the affected points. As shown in Fig. 5, the corrected phase distribution conforms well to the expected sinusoidal pattern derived in Eq. (10), thereby improving the quality of the fitting.

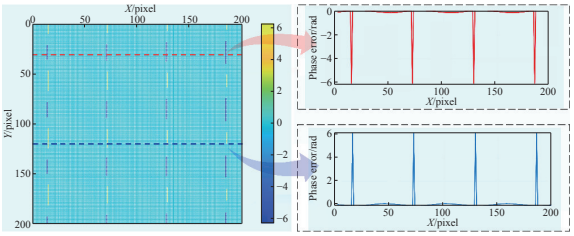

Fig. 3 Wrapped phase error distribution map before compensation.

图 3 补偿前的包裹相位误差分布图

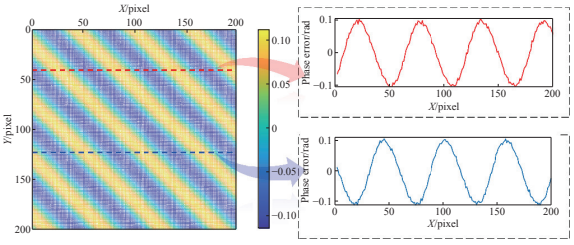

Fig. 4 Wrapped phase error distribution map after compensation.

图 4 补偿后的包裹相位误差分布图

2.4 The procedure of crosstalk calibration

The core of the proposed crosstalk correction method lies in accurately fitting the phase error map. The overall calibration procedure is illustrated in Fig. 5. The detailed steps are as follows:

Step 1: Horizontal and vertical fringe patterns are generated. Color orthogonal patterns are constructed by combining two selected color channels. Additionally, 18-step phase-shifting (PS) fringe patterns are generated in both directions.

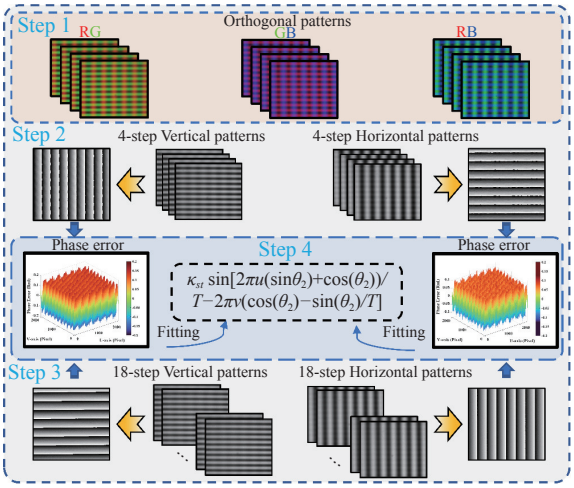

Fig. 5 Procedure of the proposed calibration method.

图 5 所提出标定方法的流程图

Step 2: The system then captures images of both the orthogonal patterns and the 18-step PS fringe patterns. Subsequently, the R, G, and B channels are separated from the captured images.

Step 3: Using the separated R, G, or B channel patterns along with the 18-step PS fringe patterns, the wrapped phase error introduced by crosstalk is computed.

Step 4: The crosstalk coefficients are calibrated by fitting the phase error map based on Eq. (10). This process is iteratively repeated from Step 2 until the full crosstalk matrix κ_{st} and θ_1 are obtained.

3 Experiment

3.1 System setup

To validate the performance of the proposed method, a prototype system for color fringe projection was constructed, as shown in Fig. 6. The system was composed of a color CMOS camera (Daheng MER2-503, 79 fps) equipped with a 25 mm lens, a color DLP projector (LightCrafter 4 500), and a personal computer. The camera-projector distance

was fixed at 750 mm, with a projection angle of 20°, and the measurement area was approximately 300 mm × 230 mm. The experiments were carried out in a laboratory environment with ambient lighting controlled at approximately 50 lux. The system was calibrated prior to measurement[20].

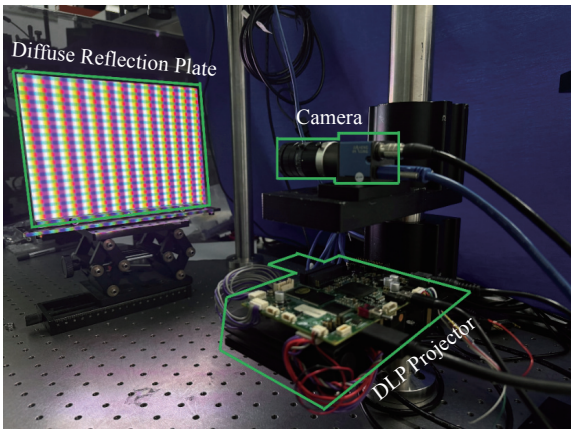

Fig. 6 CFPP system used in our experiments.
图 6 研究实验中使用的 CFPP 系统示意图

3.2 Crosstalk Coefficient Calibration Experiment

In this system, a composite fringe sequence with two orthogonal directions was first projected onto a standard diffuse whiteboard. Simultaneously, a set of twelve-step phase-shifted fringe patterns was also projected to serve as ground-truth data for calculating the wrapped phase and corresponding phase errors. All images were then sequentially captured and stored by the color camera. By separating the captured images, which contain color crosstalk, on a per-channel basis, the independent image information for each color channel could be obtained. The resulting single-channel separated images are shown in Fig. 7.

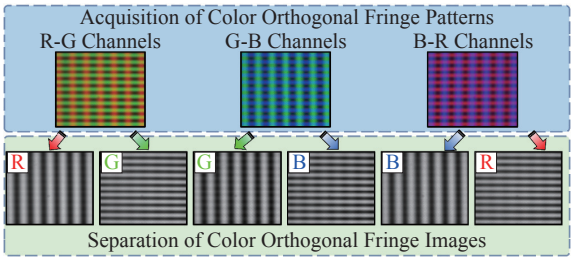

Fig. 7 Single-channel separated images containing crosstalk coefficients.
图 7 单通道分离图像(含串扰系数)

It is evident that the extent of crosstalk varies across channels due to differences in the spectral overlap regions of the color filters. Notably, significant crosstalk is observed from the red (R) channel to the green (G) channel, from the blue (B) channel to the G channel, and from the B channel to the R channel, while the reverse crosstalk effects appear relatively minor.

The phase maps were calculated from the separated single-channel fringe images and compared with the ground truth phase obtained using a 12-step reference phase-shifting method, yielding the corresponding phase error. As shown in Fig. 8, the resulting phase error distribution exhibited a directional sinusoidal pattern, with the peak amplitude directly correlated with the crosstalk coefficient κ_{st}. To balance fitting accuracy and computational efficiency, a central region of 700 × 700 pixels was selected for the optimization process based on the Particle Swarm Optimization (PSO) method, as shown in Fig. 9 and Table 1.

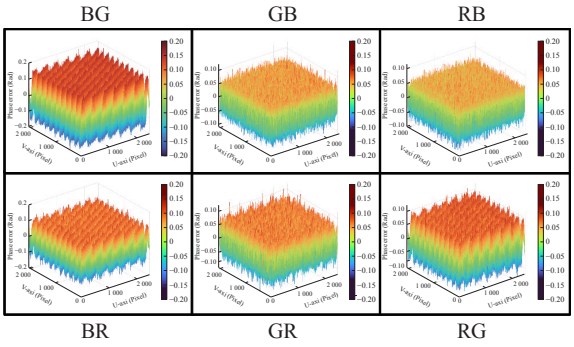

Fig. 8 Phase error distribution map of the different channels.
图 8 不同通道的相位误差分布图。

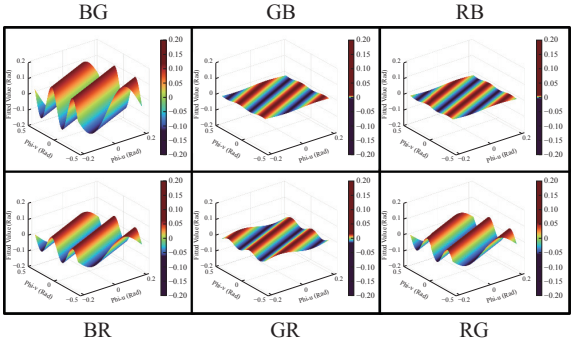

Fig. 9 The fitting results of the different channels.
图 9 不同通道的拟合结果图

Tab. 1 The Results of Crosstalk Coefficients
表 1 不同通道的串扰系数计算结果

κ_{st}	Value	R^2	κ_{st}	Value	R^2
κ_{gr}	0.0151	0.995	κ_{rg}	0.0546	0.988
κ_{bg}	0.1152	0.995	κ_{gb}	0.0546	0.998
κ_{rb}	0.0052	0.964	κ_{br}	0.0614	0.980

It can be observed that the phase errors of all channels were well fitted using the analytical model described by Eq. (10). The coefficient of determination (R^2) approached 1, confirming the accuracy and validity of the proposed phase error model.

3.3 Qualitative Experiment

Based on the calibrated crosstalk coefficients, the color crosstalk correction was performed on the original fringe images to eliminate inter-channel interference. Specifically, three images exhibiting significant crosstalk effects ($I_{G\text{with}B}$, $I_{G\text{with}R}$, and $I_{R\text{with}B}$) were selected for correction. The corresponding results after crosstalk compensation are presented in Fig. 10.

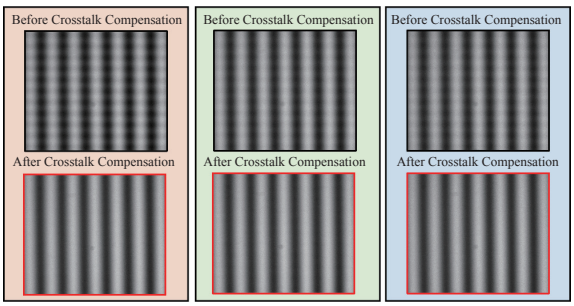

(a) $I_{G\text{with}B}$ (b) $I_{G\text{with}R}$ (c) $I_{R\text{with}B}$

Fig. 10 Phase error distribution map of different channels.
图 10 不同通道的相位误差分布图。

As shown in Fig. 10, the crosstalk responses from other channels were effectively suppressed, resulting in more accurate fringe patterns. To further validate the accuracy of the estimated crosstalk coefficients, wrapped phase maps were computed from the channel-separated images before and after correction. These phase maps were then compared against the ground truth phase values obtained from the 12-step phase-shifting method. The comparison results are illustrated in Fig. 11.

As shown in Fig. 11, a significant reduction in phase error could be observed after crosstalk compensation. The phase error distribution shifts from a structured sinusoidal pattern to a more random distribution, indicating that the phase errors caused by color crosstalk have been substantially mitigate.

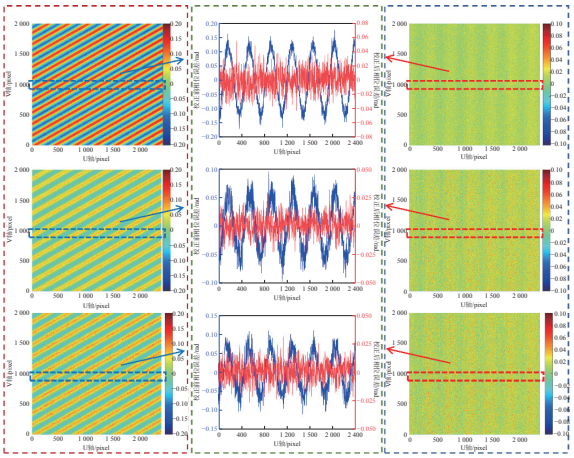

(a) (b) (c)

Fig. 11 Phase error distributions before and after crosstalk correction. (a) Crosstalk-induced phase error before correction; (b) Phase error along a selected row; (c) Residual phase error after correction.
图 11 色彩串扰校正前后的相位误差分布。(a) 校正前的串扰引起的相位误差; (b) 沿选定行的相位误差曲线; (c) 校正后的残余相位误差

3.4 Quantitative Evaluation

To quantitatively evaluate the overall accuracy of the proposed method and verify the reliability of the reconstructed 3D shape, an experiment was conducted using a standard spherical calibration plate. This plate contains two ceramic spheres with precisely known geometric dimensions, serving as ground truth for accuracy assessment. The surfaces of the spheres exhibit Lambertian reflectance properties, ensuring consistent diffuse reflection across various viewing angles. Specifically, the diameters of Sphere A and Sphere B are d_A = 31.7505 mm and d_B = 31.7391 mm, separately. And the center-to-center distance between the two spheres is s_{AB} = 60.0130 mm. In the experiment, the standard sphere calibration plate was measured at ten different spatial positions, and the final results were averaged to mitigate local noise and pose variation effects. The quantitative results are illustrated in Fig. 12 and summarized in Table 2.

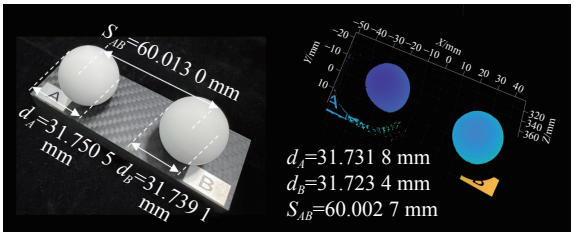

Fig. 12 Measurement results of the standard sphere calibration plate.

图 12 标准球校准板的测量结果图。

Tab. 2 Measurement results of the standard sphere calibration plate (mm)

表 2 标准球板的测量结果（毫米）

Measurement Index	Diameter d_A	Diameter d_B	Center Distance S_{AB}
1	31.728 4	31.707 8	60.013 6
2	31.723 4	31.729 8	60.014 8
3	31.736 0	31.728 3	59.986 4
4	31.752 7	31.725 8	60.004 6
5	31.732 8	31.727 3	59.998 9
6	31.728 4	31.740 4	59.994 9
7	31.728 8	31.721 8	60.014 1
8	31.722 9	31.719 4	60.017 9
9	31.730 5	31.712 7	59.991 8
10	31.734 0	31.720 8	59.989 8
Mean Result	31.731 8	31.723 4	60.002 7
MAE	0.019 1	0.016 0	0.012 0
SD	0.020 4	0.017 9	0.015 2

The measurement results indicate that the proposed parameter optimization strategy maintains high measurement accuracy, with the Mean Absolute Errors (MAE) of 0.019 1 mm, 0.016 0 mm, and 0.012 0 mm, and the corresponding Standard Deviations (SD) of 0.020 4 mm, 0.017 9 mm, and 0.015 2 mm. These results demonstrate the system's robustness and generalization capability under varying spatial configurations.

4 Conclusion

A color crosstalk calibration method based on orthogonal fringe estimators has been proposed for color fringe projection profilometry (CFPP) systems. By projecting orthogonal fringe patterns and analyzing the resulting phase errors, the crosstalk coefficients were identified through PSO-based fitting. Experimental results demonstrated that the crosstalk-induced phase distortions were significantly reduced after compensation, leading to enhanced phase accuracy and improved 3D reconstruction performance. Moreover, the entire calibration process was implemented using only commercially available components, such as standard DLP projectors and CCD cameras, which substantially reduces system cost and complexity, thereby enhancing its value for practical applications.

References:

[1] 魏鹏飞, 杜虎兵, 朱倩, 等. 基于快速迭代滤波的单帧彩色条纹投影轮廓术[J]. 中国光学, 2025, 18(5): 1097-1110.
WEI P F, DU H B, ZHU Q, *et al*.. Single-frame color stripe contour technique based on fast iterative filtering[J]. *Chinese Optics*, 2025, 18(5): 1097-1110. (in Chinese).

[2] YANG T, GU F F. Overview of modulation techniques for spatially structured-light 3D imaging[J]. *Optics & Laser Technology*, 2024, 169: 110037.

[3] FORBES A, DE OLIVEIRA M, DENNIS M R. Structured light[J]. *Nature Photonics*, 2021, 15(4): 253-262.

[4] 王张颖, 张宁宁, 高楠, 等. 基于单色条纹投影的高动态范围物体表面形貌三维测量[J]. 红外与激光工程, 2023, 52(8): 202303.
WANG ZH Y, ZHANG N N, GAO N, *et al*.. 3D surface shape measurement of high dynamic range object based on monochrome fringe projection[J]. *Infrared and Laser Engineering*, 2023, 52(8): 202303. (in Chinese).

[5] FU L N, ZHANG Z H, HUANG H, *et al*.. Three-dimensional shape measurement based on color complementary phase coding method[J]. *Optics and Lasers in Engineering*, 2024, 180: 108316.

[6] PAN J H, HUANG P S, CHIANG F P. Color phase-shifting technique for three-dimensional shape measurement[J]. Optical Engineering, 2018, 38(8): 0815005.

ZHANG Z H, LIAN X J, GAO N. Crosstalk elimination method for color composite fringe projection measuring systems[J]. *Acta Optica Sinica*, 2018, 38(8): 0815005. (in Chinese).

[7] YUAN L W, KANG J H, FENG L Y, *et al*.. Accurate calibration for crosstalk coefficient based on orthogonal color phase-shifting pattern[J]. *Optics Express*, 2023, 31(14): 23115-23126.

[8] LIU B, WANG C L, WANG S, *et al*.. Color crosstalk compensation method for color phase-shifting fringe projection profilometry based on the phase correction matrix[J]. *Optics Express*, 2024, 32(4): 5793-5808.

[9] ZHANG Z H, XU Y J, LIU Y. Crosstalk reduction of a color fringe projection system based on multi-frequency heterodyne principle[J]. *Proceedings of SPIE*, 2013, 9046: 904607.

[10] YUE M K, WANG J Y, ZHANG J S, *et al*.. Color crosstalk correction for synchronous measurement of full-field temperature and deformation[J]. *Optics and Lasers in Engineering*, 2022, 150: 106878.

[11] 邹海华, 赵宏, 周翔. 基于经验模式分解的三频彩色条纹投影轮廓术[J]. 光学学报, 2011, 31(8): 0812009.
ZHOU H H, ZHAO H, ZHOU X. Triple-frequency color-encoded fringe projection profilometry based on empirical mode decomposition[J]. *Acta Optica Sinica*, 2011, 31(8): 0812009. (in Chinese).

[12] WANG Y W, LIU L, WU J, *et al*.. Hilbert transform-based crosstalk compensation for color fringe projection profilometry[J]. *Optics Letters*, 2020, 45(8): 2199-2202.

[13] QIAN J M, FENG SH J, LI Y X, *et al*.. Single-shot absolute 3D shape measurement with deep-learning-based color fringe projection profilometry[J]. *Optics Letters*, 2020, 45(7): 1842-1845.

[14] ZHANG B W, LIN SH N, LIN J Y, *et al*.. Single-shot high-precision 3D reconstruction with color fringe projection profilometry based BP neural network[J]. *Optics Communications*, 2022, 517: 128323.

[15] 黄浩珍, 牛斌, 程深, 等. 彩色投影仪光强自适应高动态范围三维测量方法 (英文)[J]. 中国光学, 2025, 18(5): 1219-1229.
HUANG H ZH, NIU B, CHENG SH, *et al*.. Color projector light intensity adaptive high dynamic range 3D measurement method[J]. *Chinese Optics*, 2025, 18(5): 1219-1229. (in Chinese).

[16] MENON D, CALVAGNO G. Color image demosaicking: an overview[J]. *Signal Processing: Image Communication*, 2011, 26(8-9): 518-533.

[17] SUN Y, BABU P, PALOMAR D P. Majorization-minimization algorithms in signal processing, communications, and machine learning[J]. *IEEE Transactions on Signal Processing*, 2017, 65(3): 794-816.

[18] WANG D SH, TAN D P, LIU L. Particle swarm optimization algorithm: an overview[J]. *Soft Computing*, 2018, 22(2): 387-408.

[19] FENG L Y, KANG J H, LI H T, *et al*.. Rapid and flexible calibration of DFPP using a dual-sight fusion target[J]. *Optics Letters*, 2023, 48(8): 2086-2089.

Author Biographies:

FENG Lu-yuan, male, born in Heibei Province. He received the Ph.D. degree in Measurement and Control Technology and Instrument from Tianjin University, Tianjin, China, in 2025. He is currently with the China Ordnance Navigation and Control Technology Research Institute, China. His research interests include inertial navigation and vision inspection.

WU Bin, male, born in Heinan Province. He received the B.S. and Ph.D. degrees in Tianjin University, in 1997 and 2002, respectively. He is currently a Professor with the Department of Instrumentation Science and Technology, Tianjin University. His main research interests include: compute vision, object detection and vision measurement technology